Journal of Solid State Chemistry 182 (2009) 18–26

Contents lists available at ScienceDirect

Journal of Solid State Chemistry

journal homepage: www.elsevier.com/locate/jssc

Carboxylate-intercalated layered double hydroxides aged under microwave–hydrothermal treatment

P. Benito [a], F.M. Labajos [a], L. Mafra [b], J. Rocha [b], V. Rives [a,*]

[a] GIR-QUESCAT, Departamento de Quimica Inorgánica, Universidad de Salamanca, Salamanca 37008, Spain
[b] Departamento de Quimica, Universidade de Aveiro, Aveiro, CICECO, Portugal

ARTICLE INFO

Article history:
Received 23 July 2008
Received in revised form
14 September 2008
Accepted 20 September 2008
Available online 8 October 2008

Keywords:
Layered double hydroxide
Terephthalate
Ageing
Microwave

ABSTRACT

Carboxylate-intercalated (terephthalate, TA and oxalate, ox) layered double hydroxides (LDHs) are aged under a microwave–hydrothermal treatment. The influence of the nature of the interlayer anion during the ageing process is studied. Characterization results show that the microwave–hydrothermal method can be extended to synthesize LDHs with anions different than carbonate, like TA. LDH–TA compounds are stable under microwave irradiation for increasing periods of time and the solids show an improved order both in the layers and in the interlayer region as evidenced by powder X-ray diffraction (PXRD), ^{27}Al MAS NMR and FT-IR spectroscopy. Furthermore, cleaning of the surface through removal of some organic species adsorbed on the surface of the particles also occurs during the microwave–hydrothermal treatment. Conversely, although the expected increase in crystallinity is observed in LDH–ox samples, the side-reaction between Al^{3+} and ox is also enhanced under microwave irradiation, and a partial destruction of the structure takes place with an increase in the M^{2+}/M^{3+} ratio and consequent modification of the cell parameters.

© 2008 Elsevier Inc. All rights reserved.

1. Introduction

Layered double hydroxides (LDHs), also known as hydrotalcite-like compounds (HTlcs), and derived materials have a wide range of applications; they can be used as catalysts or catalyst supports, in processing of selective chemical nanoreactors, separation and membrane technology, filtration, scavening and controlled release of anions, electroactive and photoactive materials, polymer stabilizers, etc. [1,2]. They consist of positively charged brucite-type layers where a partial substitution of *M*(II) cations by *M*(III) ones has taken place; anions are, as a result, incorporated between the layers to balance the resulting excess of positive charge and water molecules also exist in the interlayer space. Intercalation of metal-containing anions and organic anions provides special characteristics to LDHs [3–5].

In previous works, some of us have studied in detail the influence of the microwave radiation on the ageing process of carbonate-containing LDHs with different lamellar compositions (Mg–Al, Mg–Cr, Ni–Al, Zn–Al, Co–Al, Co–Zn–Al, Zn–Ni–Al) [6–10]. A fast improvement of the crystallinity and a modification of the textural and thermal properties of the solids after the microwave–hydrothermal treatment were found. Furthermore, it was also possible to avoid ZnO segregation in zinc-containing systems [10] and cobalt oxidation in Co,Al compounds [8]. Taking into account the successful results obtained, the next step was to study the mutual effect of the nature of the anions located within the layers and the microwave-ageing process. Hussein et al. [11] have previously reported the intercalation of anionic surfactant dodecyl sulphate and naphthaleneacetate into a Zn–Al LDH, concluding that the nanocomposite can be synthesized faster by the microwave-assisted method than by the conventional one. They also observed that by using the microwave-assisted method, a slightly larger amount of Al^{3+} ions could be incorporated into the layers. However, the effect of the microwave radiation on the synthesis process of LDH–carboxylates has not been reported so far.

Carboxylate anions have been already intercalated in LDHs. Different types of carboxylate anions, with one or two carboxylic functional groups and with aliphatic or aromatic hydrocarbon chains, have been intercalated. Since the first synthesis reported by Drezdzon [12], the complexity of the anions intercalated has increased; LDHs containing interlayer carboxylate anions have attracted considerable attention in recent years, as these materials have a number of interesting properties and potential applications [13–16]. In addition, several studies have been carried out to gain information about the structure of the interlayer region where carboxylate anions are inserted [17–23], the enthalpies of ion exchange of dicarboxylate anions [24] and the kinetics and mechanism of the intercalation process [25]. In summary, it has been found that the interlayer spacing of dicarboxylates varies

* Corresponding author. Fax: +34 923 29 45 74.
E-mail address: vrives@usal.es (V. Rives).

0022-4596/$ - see front matter © 2008 Elsevier Inc. All rights reserved.
doi:10.1016/j.jssc.2008.09.015

linearly with the length of the chain for linear aliphatic dicarboxylates [26], while for aromatic carboxylates two arrangements can be attained, namely, either perpendicular or parallel to the layers, mostly depending on the lamellar charge [27] and the hydration degree [18]. Several synthetic routes can be followed to prepare this kind of materials: direct ion exchange, coprecipitation, rehydration, thermal melting reaction, preswelling with glycerol [4,28] and addition of the carboxylic acid followed by precipitation of the product by addition of the mixture to a basic solution [29].

In the present work, two carboxylate species were chosen, oxalate (ox) ($C_2O_4^{2-}$) and terephthalate (TA) (C_6H_4-1,4-$(COO^-)_2$). The former is a small anion only constituted by two carboxylate groups, while the latter is also a dicarboxylic anion, but with an aromatic ring. One of the most important properties of ox anions is their complexation ability toward metallic cations, which is used in the so-called ox process. Metal oxalates are used as precursors for preparing metal oxide nanoparticles using controlled thermal decomposition; mixed oxides have been also prepared from LDHs [30,31] since carboxylate anions can react with the layer cations. However, this reactivity can be a drawback during the synthesis of the compounds. On the other hand, the synthesis of TA-intercalated materials is not a difficult task, but it usually takes several hours with vigorous stirring at room or moderate temperatures [12]; when carried out at higher temperatures and pressures, although the solids show the same structure at room temperature structure, they are thermally unstable [32]. In some cases, TA anions are merely used for swelling the interlayer space for an easier incorporation of larger polyoxometallate anions [33–36], and then pillaring of the polyoxometalates can occur in an already expanded structure.

2. Experimental

2.1. Synthesis of LDH–carboxylate

The synthesis of the samples intercalated with TA or ox anions is carried out following the coprecipitation method at constant pH. A given amount of the carboxylic acid (terephthalic or oxalic) is dissolved under heating at moderate temperatures and increasing the pH until a value of 7 in the case of the Zn,Al series and of 10 for the Mg,Al systems is reached. Once the acid is completely dissolved, a solution containing the metal cation salts is added drop wise. The pH is maintained constant by addition of a NaOH solution. All the systems are kept under nitrogen atmosphere and the water used to prepare the solutions had been previously boiled and cooled bubbling nitrogen in order to avoid carbonate contamination. Once the addition is complete the slurry is divided into several aliquots, which are submitted to different ageing treatments in a Milestone ETHOS PLUS Microwave oven working at 2.45 GHz. Digestion vessels of a volume of 100 ml filled with 50 ml of slurry per vessel are used. They are sealed and mounted on the turntable in the microwave. An initial temperature program is established before reaching the desired temperature [6]: 3 min up to 85 °C, 2 min at 85 °C, and 3 min up to 125 °C for the magnesium-containing samples and up to 100 °C for those with Zn to avoid segregation of the non desired ZnO phase [10]. The treatment is extended at the selected temperatures for 10, 30 and 180 min. The temperature is measured by a thermocouple introduced in the reference vessel. The software dynamically controls the temperature profile adjusting the delivered power in every moment. A feedback mechanism optimizes the effects of too high temperature and pressure and at the same time, prevents thermal runaways. The samples are named as follows: XA-Y-HWt, where $X = M$ (Mg) or Z (Zn), $Y =$ TA or ox and t is the ageing time (min). The non-aged samples (or fresh sample) are named as XA-TA-0 or XA-ox-0. In ZA samples, a number 1 is placed at the beginning of the name to indicate ageing at 100 °C, i.e. 1ZA-TA-HW10.

2.2. Techniques

Element chemical analysis for Mg, Al and Zn is carried out by atomic absorption in a Mark 2 ELL-240 apparatus, in Servicio General de Análisis Químico Aplicado (University of Salamanca, Spain), while the carbon content is determined in an Elemental Analyzer Leco SHCN-932, in Servicio Interdepartamental de Investigación (Sidi, University Autonoma of Madrid, Spain).

Powder X-ray diffraction (PXRD) patterns are recorded in a Siemens D-500 instrument using Cu$K\alpha$ radiation ($\lambda = 1.54050$ Å) and equipped with Diffrac AT software. The data are collected in the 2–70° (2θ) range with a 0.05° (2θ) step and a 1.5 s per step counting time. Identification of the crystalline phases is made by comparison with the JCPDS files [37]. The crystallite size is calculated by the Scherrer equation from the FWHM of the (003) and (006) diffraction lines using the Warren correction.

The FT-IR spectra are recorded in a Perkin-Elmer FT1730 instrument, using KBr pellets; 100 spectra (recorded with a nominal resolution of 4 cm^{-1}) are averaged to improve the signal-to-noise-ratio.

Specific surface area assessment is carried out in a Gemini instrument from Micromeritics. The sample (ca. 80–100 mg) is previously degassed in flowing nitrogen at 110 °C for 2 h in a FlowPrep 060 apparatus, also from Micromeritics, in order to remove physisorbed water and the data are analysed using published software [38].

^{27}Al MAS NMR spectra are recorded on Bruker Avance 400 spectrometer at 104.3 MHz using short, 0.6 μs (equivalent to 10°) radio-frequency pulses, 1 s recycle delay and 15 kHz spinning rates. Chemical shifts are quoted in ppm from $Al(H_2O)_6^{3+}$. The ^{13}C CP/MAS NMR spectra are recorded at 100.61 MHz, using 4 μs ^{1}H 90° pulses, a contact time of 2 ms, a 5 s recycle delay and a 9 kHz spinning rate. Chemical shifts are given in ppm from TMS.

The triple-quantum ^{27}Al MAS NMR spectrum is recorded using the Z-filter three-pulse sequence. The lengths of the first and second hard pulses (radio-frequency magnetic field amplitude $\nu = 150$ kHz) are 3.4 and 1.1 μs, respectively [39]. The length of the third soft pulse ($\nu = 10$ kHz) is 11 μs. The MAS rate (ν_r) is 15 kHz. One hundred and forty-two points are acquired in the t1 domain in increments of $1/\nu_r = 67$ μs. The ppm scale of the sheared spectrum is referenced to ν_0 frequency in the ν_2 domain and to 1.42 ν_0 (high-resolution spectra after shearing) in the ν_1 domain (reference $Al(H_2O)_6^{3+}$).

3. Results and discussion

3.1. Powder X-ray diffraction (PXRD)

PXRD patterns of the samples with TA are shown in Fig. 1. The basal spacing of the first peak around 14 Å indicates that the TA anions are forming a monolayer with the benzene rings perpendicular to the layers, an orientation favoured by a high-layer charge and a large interlayer water content [18]. No AlOOH reflections are recorded for the samples hydrothermally treated for short periods of time, but the diffraction pattern for sample MA-TA-HW180 shows two extremely weak peaks corresponding to an unknown phase [32]. The non-basal diffraction lines are broad and non-symmetric and the shape of the peaks around 60° is characteristic of LDHs containing large anions in the

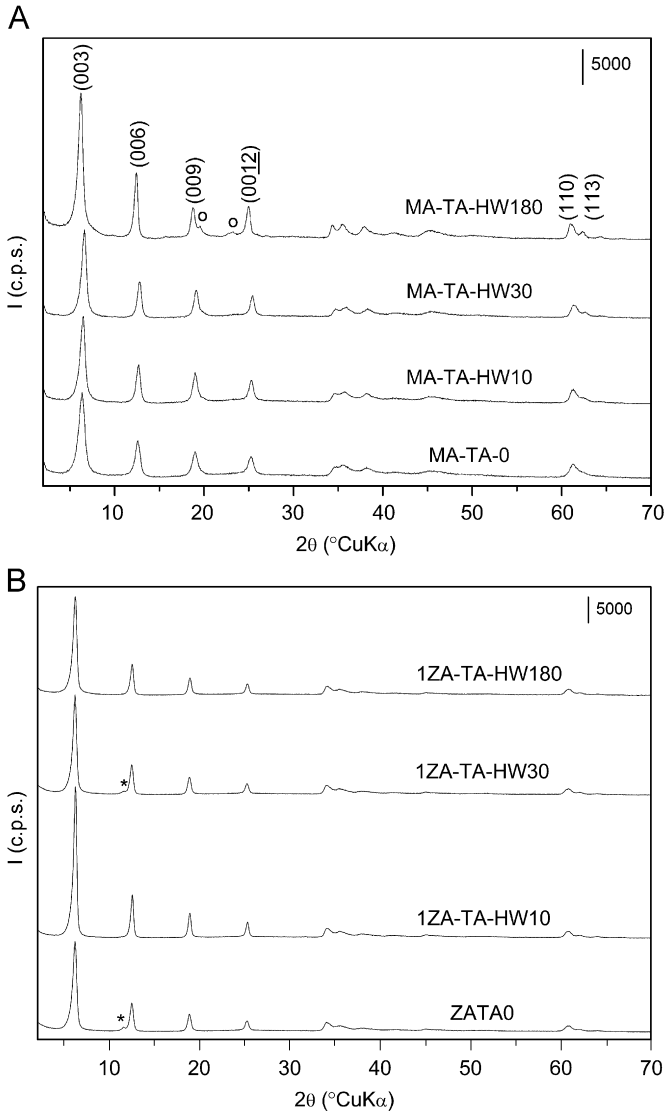

Fig. 1. PXRD patterns of the synthesized samples, MA-TA series (A) and ZA-TA series (B) (0: unknown phase * LDH–CO_3).

interlamellar region. The observed *d*-spacings may also vary slightly depending on the preparation method, mainly due to different hydration degrees of the samples [28].

Concerning the Mg,Al series, the pattern of the fresh sample is quite similar to those of the samples irradiated for short periods of time and it is necessary to extend the microwave treatment up to 180 min in order to appreciate a considerable increase in the intensity of the basal diffraction lines. Crystallite sizes are calculated by the Scherrer equation and the values determined are summarized in Table 1. An enlargement of the coherent domain in the *c* direction is attained in 10 min of microwave treatment, which remains constant until a 180 min treatment is applied. Although an improvement in the crystallization degree is not detected in solids irradiated for short periods of time, a reduction in the basal spacing takes place, achieving short values such as 13.34 Å for sample MA-TA-HW30. These values are similar to those reported by Jones et al. from a simulated swelling curve for Mg_2Al(TA) with ca. 34 water molecules per formula [18]. The diffraction lines due to planes (110) and (113) around $2\theta = 60^\circ$ become resolved as the irradiation time is prolonged. The *a*-lattice parameter determined for the non-aged sample is 3.02 Å and it increases only very slightly with the irradiation time.

Table 1
M^{2+}/M^{3+} and TA/Al^{3+} molar ratios, lattice parameters (*c*′ and *a*, Å) and crystallite size (*D*, Å) for MA-TA and ZA-TA samples

Sample	M^{2+}/M^{3+}	TA/Al^{3+}	*c*′	*a*	*D*
MA-TA-0	2.19	0.47	13.88	3.024	110
MA-TA-HW10	2.13	0.46	13.66	3.020	140
MA-TA-HW30	2.16	0.48	13.34	3.016	150
MA-TA-HW180	2.29	0.52	14.17	3.030	220
ZA-TA-0	2.04	0.56	14.12	3.048	190
1ZA-TA-HW10	2.08	0.58	14.01	3.044	250
1ZA-TA-HW30	2.24	0.67	14.11	3.044	200
1ZA-TA-HW180	2.14	0.63	14.06	3.044	190

A small diffraction line due to a carbonate-intercalated phase is observed for some samples of the ZA system, but since it does not follow a defined trend, it can be ascribed to a contamination of the samples by atmospheric CO_2 during the washing process, because of the high affinity of these materials for this species. Nevertheless, this series of samples show an anomalous behaviour if compared to the MA series: the sample submitted to the longest microwave irradiation treatment does not show the sharpest and most intense peaks, which is actually observed for the sample irradiated for 10 min. In other words, contrary to the findings for the MA series, a steady increase of the crystallinity degree for the ZA samples is not observed when the irradiation time is increased. It seems that the solids are able to achieve a well ordered structure in a short microwave treatment, and after that no additional improvement is observed, a hypothesis supported by the variation in the crystallite size, Table 1. However, this behaviour is similar to that observed for Zn,Al–CO_3 compounds aged under a microwave–hydrothermal treatment and it was attributed to the finite Ostwald ripening [10].

A closer inspection of the basal spacing values for the different samples, Table 1, indicates that they do not follow any well defined trend. The decrease observed for sample 1ZA-HW10 can be related to the improved crystallinity of this sample: the interlamellar region is well ordered and the electrostatic interactions between anionic species and hydroxyl layers become enhanced, decreasing the *c* parameter. At longer irradiation times two facts must be considered: during microwave heating a larger amount of water molecules can be packed in the interlamellar region [40] increasing the basal space [18]; moreover, the Zn/Al ratio is slightly modified (see below) altering the layer–interlayer interactions. Finally, values for parameter *a*, around 3.04 Å, are larger than those above reported by the MA-TA samples.

PXRD patterns of the samples intercalated with ox are shown in Fig. 2. They are characteristic of LDHs containing ox anions oriented parallel to the layers adopting an arrangement like that for CO_3^{2-}. In this configuration, ox groups are hydrogen-bonded to both adjacent hydroxylated planes via their four oxygen atoms [30], with basal spacings around 7.7 Å. However, a deeper inspection of the patterns reveals that, together with the expected fast enhancement of the crystalline degree with the microwave treatment, the basal spacing increases with the irradiation time, see Table 2. On predicting guest orientations in LDHs, Fogg et al. [21] found that if the main axis of the ox anion is parallel to the layers, an optimized structure with the anions orienting their molecular planes essentially perpendicular to the layers would be obtained; this would give rise to an increase in the interlamellar space. Thus a partial reorientation of the ox anions would be possible during the ageing treatment, aiming to achieve an optimized structure and yielding larger basal spacings. Nevertheless, as it has been written above, not only the arrangement of

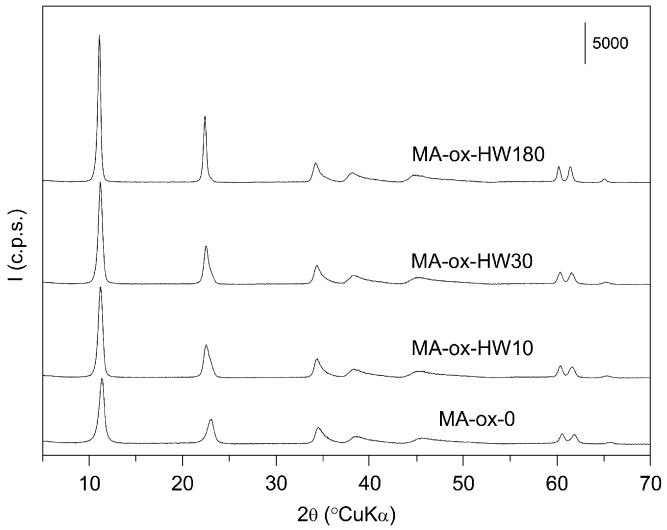

Fig. 2. PXRD patterns of the samples containing oxalate anions.

Table 2
M^{2+}/M^{3+} and ox/Al^{3+} ratios, lattice parameters (c' and a, Å) and crystallite size (D, Å) for MA-ox samples

Sample	M^{2+}/M^{3+}	ox/Al^{3+}	c'	a	D
MA-ox-0	2.67	0.61	7.78	3.058	145
MA-ox-HW10	2.91	0.61	7.89	3.066	165
MA-ox-HW30	3.37	0.53	7.89	3.068	190
MA-ox-HW180	3.63	0.66	7.94	3.072	260

the anions, but also the amount of water, the chemical composition of the layers (see below) and the layer–interlayer electrostatic interactions can modify the distance between two adjacent layers.

3.2. Element chemical analysis

The M^{2+}/M^{3+} experimental ratio for all TA-containing samples is slightly large, but close to the expected one; the values are summarized in Table 1. Values of 2.19 and 2.04 are obtained for samples MA-TA-0 and ZA-TA-0, respectively, so it can be concluded that the coprecipitation takes place almost quantitatively. Differences in the Mg/Al molar ratio are very small from one sample to another. The largest difference (lower, however, than 10% if compared with the untreated sample) is observed for sample 1ZA-TA-HW30.

On the other hand, among the ox-samples, Table 2, sample MA-ox-0 shows an experimental Mg^{2+}/Al^{3+} ratio larger than two. Furthermore, the longer the irradiation time, the larger the M^{2+}/M^{3+} ratio value. In this case, release of aluminium cations from the hydrotalcite structure takes place in a greater extent, and the Mg^{2+}/Al^{3+} value reaches values as large as 3.63. This large deviation from the expected value even for the just coprecipitated sample is related to the formation of $[Al(C_2O_4)_3]^{3-}$ complexes which remain in solution, because of the reactivity of interlamellar $C_2O_4^{2-}$ anions with metallic species of the brucite-type layers [30]. This reactivity is even enhanced by the microwave post-treatment, thus considerably decreasing the stability of the structure. These results allow us to explain the values of the increase of c and a cell parameter above reported. The lower content of Al^{3+} leads to weaker layer–interlayer electrostatic interactions and larger basal spacings. Moreover, the release of Al^{3+} cations having smaller atomic radius leads to the increase in the value of a.

The amount of organic anion is calculated from carbon elemental analysis, assuming that only TA and ox anions contribute to the carbon content in each series of samples. For LDHs–TA, on the average, the samples contain ca. 1.5–2 mol of C per formula, which corresponds to ca. 0.14–0.16 mol of TA ($C_6H_4(COO)_2^{2-}$) per formula, Table 1. For all samples the amount of TA anions is quite close to that required to balance the positive charge of the layers. A slight increase of the ratio is observed along the irradiation time. The variations in the chemical composition could be due to the presence of TA anions adsorbed on the external surface of the crystallites, although the presence of carbonate anions (contamination from atmospheric CO_2 during handling of the samples) together with the organic species cannot be excluded. Similarly, the calculated amount of ox anions, Table 2, almost coincides with the amount required to balance the positive charge originated by the trivalent aluminium species in the layers.

3.3. ^{27}Al MAS NMR

The ^{27}Al MAS NMR spectra of samples MA-TA (Figs. 3, 4 and supplementary information Fig. 1) are similar to those reported previously for Mg,Al–CO_3 LDHs, displaying a main peak at ca. 9.7 ppm (Al1) and a broad low-frequency shoulder (Al2), both assigned to octahedral Al species [41]. The presence of two resonances is confirmed by 3Q ^{27}Al MAS NMR (Fig. 4A). It is interesting to notice that with increasing irradiation times the intensity of the broad Al2 peak monotonously decreases and is essentially absent after 180 min. The Al2 resonance is related to a site with a larger quadrupole coupling constant, corresponding to relatively distorted local Al environments, while Al1 has been attributed to a distribution of Al environments generated by the random insertion of Al in the layers [41]. Thus, it seems that irradiation restores the local symmetry of some Al environments, which is consistent with the improved crystallinity of samples, revealed by PXRD.

The ^{27}Al MAS NMR spectra of samples ZA-TA also displays two resonances, Al1 and Al2, at, respectively, ca. 11 and 14 ppm (Figs. 3, 4 and supplementary information Fig. 2). The Al2 peak is stronger for the non-irradiated sample and weaker for the most crystalline sample, after 10 min irradiation, for which Al1 dominates. The samples irradiated for longer times again exhibit less intense Al1 peaks. However, it is interesting to point out that, unlike the MA series, ZA-TA samples always contain the, more distorted (large quadrupole coupling constant) Al2 site.

All ^{27}Al MAS NMR spectra of MA-ox samples (including the non-irradiated one) display a single peak at ca. 9.3 ppm attributed to the Al1 site (supplementary information Fig. 3). The FWHM of this resonance is in the range 303 (non-irradiated) to 293 Hz (180 min irradiation), much sharper than the one reported for Mg,Al–CO_3 (370 Hz) [41]. This is accord with the PXRD evidence.

3.4. ^{13}C CP/MAS NMR

The ^{13}C CP/MAS NMR spectra provide information about TA anions located in the interlamellar region, and also inform about the possible contamination by carbonate anions. The ^{13}C CP/MAS NMR spectra of samples MA-TA-HW-180 and 1ZA-TA-HW10 are shown in Fig. 5. Three peaks are expected, corresponding to the three types of unequivalent carbon atoms in the TA molecule. Similar shifts are recorded for both samples: the unsubstituted aromatic carbons, C^1, give rise to a peak at 128 ppm, the C^2 carbon is associated to the signal at 136 ppm, and the resonance peak at 173 ppm is attributed to the carbon from the carboxylate anion,

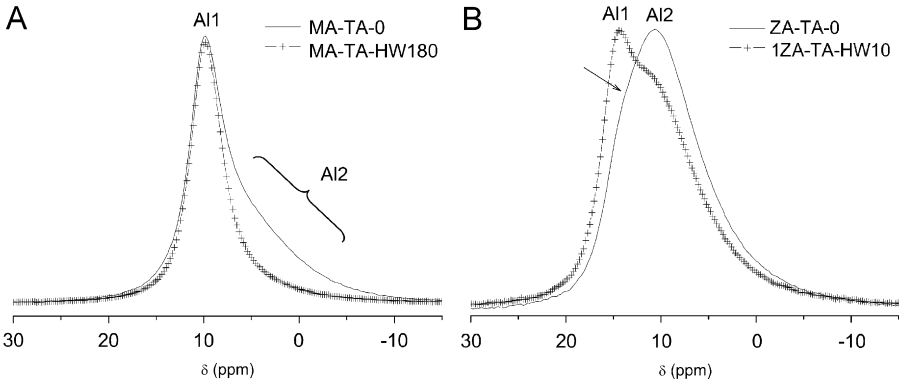

Fig. 3. ^{27}Al MAS NMR spectra of fresh samples (not aged) and solids aged for 180 min of MA-TA (left) and ZA-TA series (right).

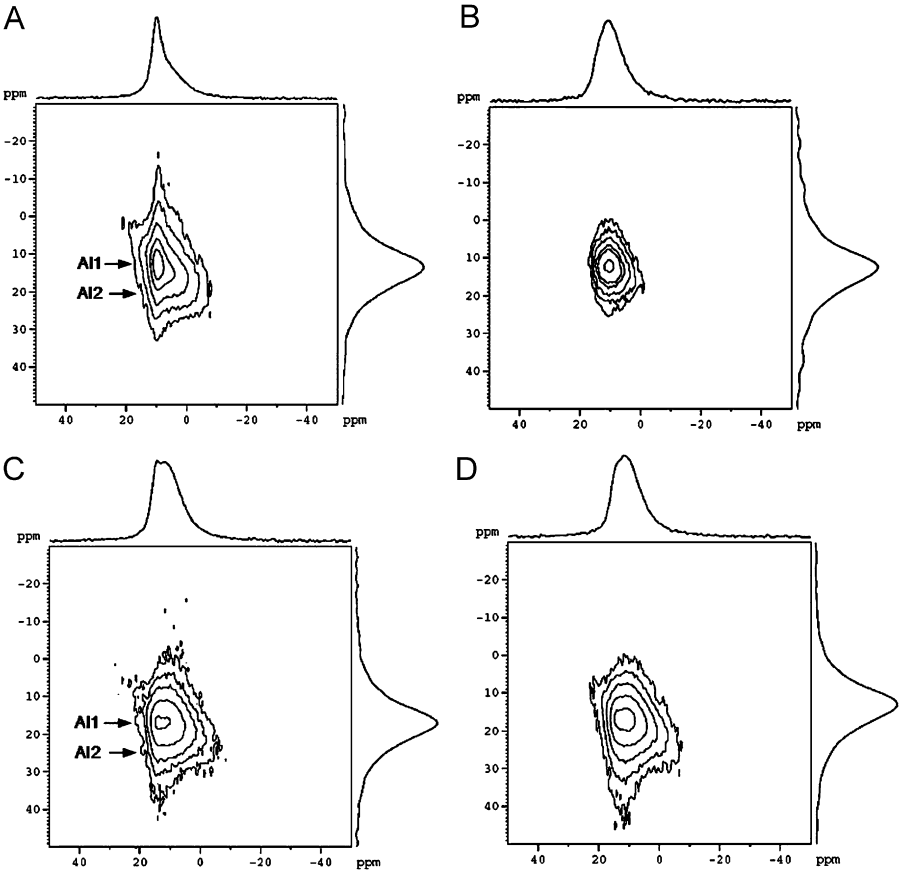

Fig. 4. 3Q ^{27}Al MAS NMR spectra of samples MA-TA-HW30 (A), ZA-TA-0 (B), 1ZA-TA-HW10 (C) and 1ZA-TA-HW30 (D).

C^3. In addition, the faint resonance at 170 ppm for sample MA-TA-HW180 is ascribed to residual carbonate.

The carboxylate carbon peak is more intense for the ZA sample than for the MA one (Fig. 5). The cross-polarization technique involves a magnetization transfer from nearby protons to the carbon nucleus under investigation providing a signal enhancement and the intensity of the peak is directly related to the amount of nearby ^{1}H atoms from which the magnetization is transferred. Thus, it seems that the carboxylate groups in the ZA samples are surrounded by a larger amount of hydrogen atoms than in the MA samples, well from interlayer water molecules or from lamellar hydroxyl groups. Most of the interlayer water molecules in these samples form a monolayer on each of the hydroxide surfaces and are generally excluded from the hydrophobic midplane of the interlayer formed by the phenyl rings of the anions [20]. The PXRD patterns reveal a higher crystallinity degree for the ZA samples than for the MA ones, a fact that implies a better ordered interlamellar region as well. Consequently, if all the water molecules are located close to the carboxylate groups, a larger amount of hydrogen bonds can be formed between them, as in carbonate containing LDHs and the amount of hydrogen atoms able to transfer magnetization will be larger. In addition, as the crystallinity degree is higher, the layer–interlayer electrostatic interactions can be enhanced as well. However, the electrostatic interaction between the carboxylate species and the hydroxyl layer would, in principle, weaken the electrophylic character towards the carbon atom, shifting the position of the peak, but in our case this behaviour is not observed [42].

The ^{13}CP/MAS NMR spectra of samples MA-ox-0 and MA-ox-HW300 (supplementary information Fig. 4) show a single

resonance peak close to 171 ppm attributed to the carboxylate groups, as no aliphatic carbons exist in the molecule. This peak slightly shifts to lower ppm from sample MA-ox-0 to MA-ox-300.

3.5. FT-IR spectroscopy

The FT-IR spectra also confirm the intercalation of TA anions within the interlamellar region, Fig. 6, and although these anions are intercalated in the gallery space, their vibrational modes are similar to those of unperturbed TA, with only subtle differences in the positions of the peaks. Furthermore, the absence of absorptions close to 1700 cm^{-1}, characteristic of the presence of free acid species, confirms that only the anion is present. The two strong, rather sharp peaks located close to 1560 and 1390 cm^{-1} are due to stretching vibrations of the $-COO^-$ group of the anion (1575 cm^{-1}, ν_{as}(OCO); 1380 cm^{-1} ν_s(OCO)); and the two medium-strong peaks at 818–821 cm^{-1} and 739–745 cm^{-1} are due to the vibrations of the benzene ring (823 cm^{-1}, γ(CH); 745 cm^{-1}, δ(CC)). The deformation vibration mode of water molecules, which is normally observed in the spectra of LDH compounds, is obscured by the very intense band of the antisymmetric stretching vibration.

Some changes are observed in the 1550–1350 cm^{-1} range of the spectra for both series of samples. The fresh sample in the MA series, MA-TA-0, shows very intense peaks due to the organic component. However, for the sample irradiated for just 10 min, a decrease in the intensity of these bands takes place, but they remain in their original positions, and the band due to the water bending mode is more easily detected. Finally, by prolonging the ageing treatment, the intensities of the bands are enhanced. It can be assumed that TA anions are adsorbed on the surface of the unaged sample, but during the microwave–hydrothermal treatment the surface is cleaned and a higher amount of anions is incorporated into the interlamellar region, in agreement with the specific surface area values (see below). For the zinc containing samples, nevertheless, a change in the relative intensity of the bands due to the carboxylate group is observed. Although no carbonate band is observed, the close position of the band due to the symmetric mode of the $-CO_2^-$ moiety of the TA and the $\nu_3(CO_3^{2-})$ mode makes quite difficult to confirm its absence.

In order to gain information about the interaction between TA anions and the brucite-type layers, the difference (Δ) between the positions of the bands due to the ν_{as} and ν_s vibrational modes of TA was calculated, Table 3. A value of 182 cm^{-1} is obtained for MA-TA-0 and MA-TA-HW10 samples, but when the irradiation time is increased the difference between the positions of these bands decreases to 170 cm^{-1}. On the other hand, regarding zinc-containing samples, a smaller difference is calculated for the fresh sample, 176 cm^{-1}, but for this series the value of Δ is reduced even for short irradiation times, then it slightly increases again, reaching a constant value of 166 cm^{-1}. The variation in Δ is related to the modification of the carboxylate coordination, and a value of Δ close to 170 cm^{-1} is characteristic of a symmetric coordination of the $-CO_2^-$ group within the interlayer region. That is, the larger the irradiation time, the larger the order in the interlayer, giving rise to a symmetric coordination of carboxylate species [5].

In addition, the OH stretching band is recorded around 3430 and 3410 cm^{-1} for series MA-TA and ZA-TA, respectively. The shift towards lower wavenumbers suggests stronger electrostatic interactions between the layers and the anionic species. This band is broader than in carbonate containing samples, probably

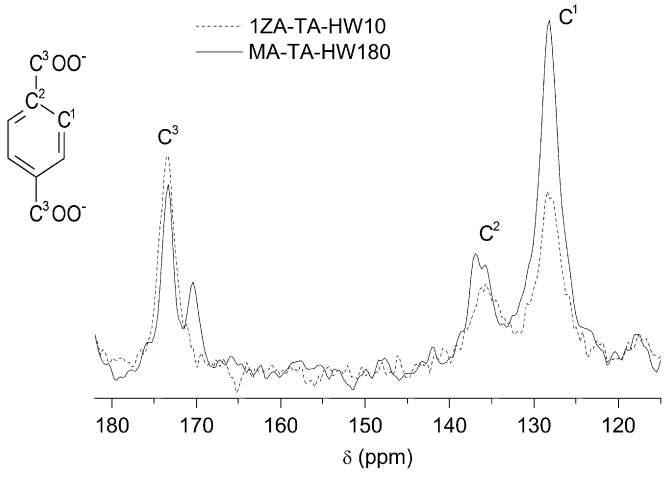

Fig. 5. ^{13}C CP/MAS NMR spectra of samples MA-TA-HW180 and 1ZA-TA-HW10.

Table 3
Positions (cm^{-1}) of the bands due to vibrational modes, ν_{as}(OCO) and ν_s(OCO), of TA anions and their difference $\Delta = \nu_{as} - \nu_s$

Sample	ν_{as}(OCO)	ν_s(OCO)	Δ
MA-TA-0	1568	1386	182
MA-TA-HW10	1572	1390	182
MA-TA-HW60	1568	1392	176
MA-TA-HW180	1564	1394	170
ZA-TA-0	1562	1386	176
1ZA-TA-HW10	1562	1398	164
1ZA-TA-HW30	1562	1396	166
1ZA-TA-HW60	1562	1396	166
1ZA-TA-HW180	1562	1396	166

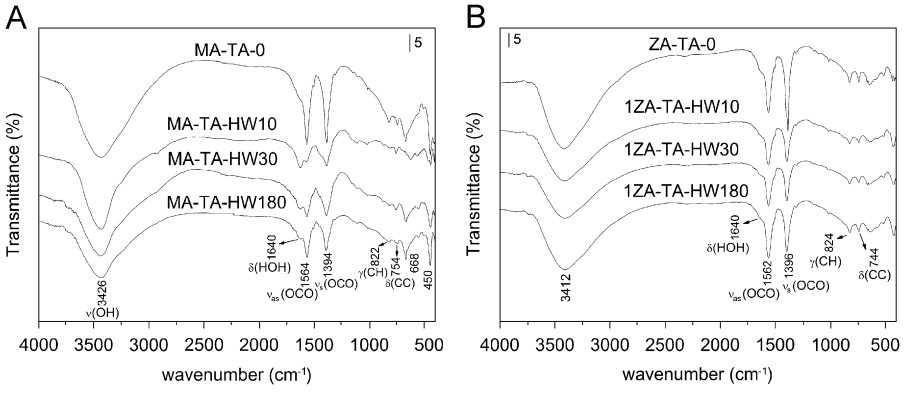

Fig. 6. Evolution of the FT-IR spectra along microwave ageing for MA-TA (left) and ZA-TA (right) samples.

due to the existence of hydrogen-bonded hydroxyl groups with different strength, with participation of carboxylate groups of the TA anion [43].

The FT-IR spectra of MA-ox samples are shown in Fig. 7. Although bands due to the LDH structure and to ox groups are observed, they are modified in comparison to those for pure LDHs and ox anions. Furthermore, the shape of the bands is slightly modified during the treatment. It should be first noticed that molecular vibrations of the ox anion are very sensitive to its symmetry and to the nature of the interactions between $C_2O_4^{2-}$ and its environment, through hydrogen or coordination bonds; the FT-IR spectra of ox anions is dependent on the ox complexes formed [44]. In this case, the ν_{as} (OCO^-) band appears in the same position as that for TA compounds (overlapped with the δ_{HOH} mode); whereas the ν_s(OCO^-) band splits into two bands 1380 and 1302 cm^{-1}, and a new ν_s(OCO^-) stretching band at 1436 cm^{-1} is observed [30]. Such changes account for a fundamental modification of the D_{2h} symmetry of $C_2O_4^{2-}$. Regarding the effect of the microwave radiation on the spectra, it should be noticed that an inversion in the relative intensity of the former peaks is observed for the MA-ox-HW180 sample. This could be related to an increase in the intensity of the band at 1380 cm^{-1} of the ox group, but it should be taken into account that the $\nu_3(CO_3^{2-})$ band is recorded in this range as well, so if some CO_3^{2-} exist in the interlayer, the decrease in the intensity of this peak could be equally related to a release of contaminating CO_3^{2-} anions.

In addition, the broad band due to $\nu_{(OH)}$ vibration modes is rather different from those previously reported; it is shifted towards higher wavenumbers and it is possible to distinguish different minima in the broad peak. This behaviour is similar to that observed by Wypich et al. [45] upon intercalation of mono and dicarboxylic acids in zinc hydroxide nitrate. Finally, the low-wavenumber region, where lattice vibrations of the layers are recorded, is quite different from that for carbonate-intercalated compounds. A broad and intense band with several shoulders is recorded for all compounds, whatever the aging time, with a minimum at ca. 600 cm^{-1} instead of 800 cm^{-1}. The lower intensity of the band at 800 cm^{-1} was previously ascribed to a high ordering of the interlayer domains with a low-water molecules content, and to strong interactions between interlayer anions and layer hydroxyl groups [45].

From these results it could be concluded that ox anions strongly interact with brucite-type layers altering the symmetry of the anions and the structure of the layers, in agreement with results previously obtained by other authors [5]. In our case it is also observed that the interactions change with the microwave aging.

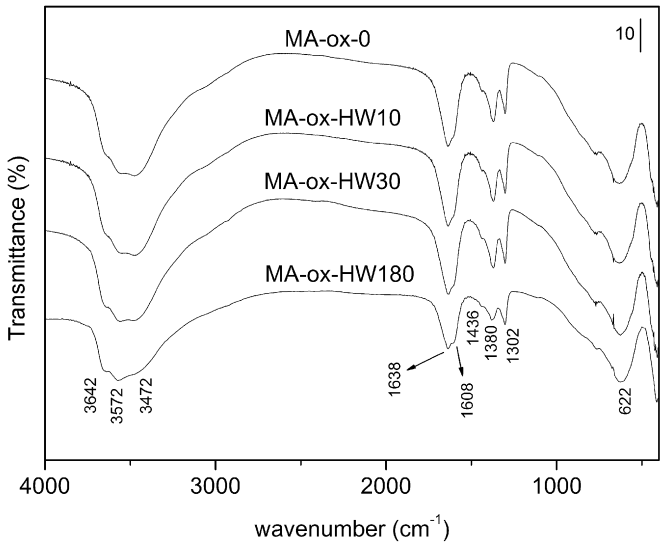

Fig. 7. Evolution of the FT-IR spectra along microwave ageing for MA-ox samples.

3.6. N_2 adsorption/desorption at −196 °C

The specific surface area values for the samples studied are shown in Table 4. Appreciable differences are observed depending on the layer composition. For the magnesium compounds (MA-TA), both the fresh sample (MA-TA-0) and those irradiated for short periods of time (MA-TA-HW10, MA-TA-HW30) do not present any measurable surface area, that is, the value should be below the detection limit of the instrument used. Nevertheless, for the sample aged for a longer period of time, MA-TA-HW180, despite the higher crystallinity degree of the compounds which would imply a larger particle size and a cancellation of the area accessible to the nitrogen molecules, a slight surface development is observed. This behaviour could be related to the cleaning of the surface during the microwave–hydrothermal treatment and removal of some organic species adsorbed on the surface of the particles. However, the presence of an amorphous phase, could be also the responsible of the increased S_{BET} value. Conversely, the zinc containing samples (ZA-TA) show considerably higher specific surface areas.

The inclusion of TA anions in the interlayer region does not significantly modify the textural properties of the solids, and isotherms (not shown) similar to those recorded for carbonate containing compounds are recorded. They belong to Type IIb of the Rouquerol classification, being characteristic of lamellar compounds with slide-shaped interparticle pores [46]. Almost parallel adsorption/desorption branches are observed for the zinc containing solids, while a broader hysteresis loop is recorded for the MA-TA samples. Regarding the effect of the microwave–hydrothermal treatment on the shape of the isotherm and the hysteresis loop, no important differences are observed among the different samples, and only a slight decrease of the width of the hysteresis loop can be noticed.

The intercalation of large anions within the interlayer space could give rise to development of microporosity. However, different studies carried out on the porosity of pillared LDHs indicated that development of porosity in this kind of materials is not evident [47]. The *t*-plots were used to qualitatively study the presence of micropores in our TA-intercalated samples, Fig. 8. Extrapolation of the straight lines of the *t*-plot for the MA-TA sample passes through the origin, in agreement with the presence

Table 4
Specific surface area (S_{BET}, $m^2 g^{-1}$), micropore surface area (S_μ, $m^2 g^{-1}$) and pore volume (V_p, $ml g^{-1}$) of MA-TA, 1ZA-TA and MA-ox samples

Sample	S_{BET}	S_μ	V_p
MA-TA-0	–	–	–
MA-TA-HW10	–	–	–
MA-TA-HW30	–	–	–
MA-TA-HW180	8	2	31.9
ZA-TA-0	61	26	82.1
1ZA-TA-HW10	44	16	60.6
1ZA-TA-HW30	56	22	73.8
1ZA-TA-HW180	45	16	54.8
MA-ox-0	46	-	187.2
MA-ox-HW10	41	-	114.4
MA-ox-HW30	35	-	91.3
MA-ox-HW180	22	-	47.8

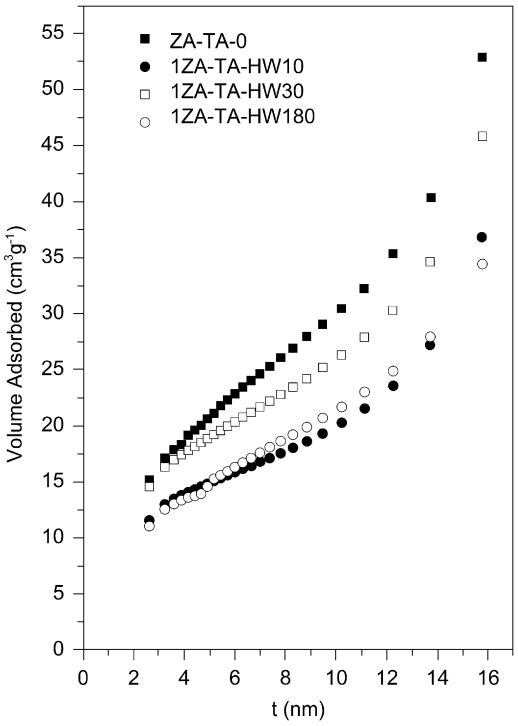

Fig. 8. *t*-plots of ZA-TA samples.

of mesoporous and the absence of micropores. However, the *t*-plot suggests the presence of micropores for the zinc-containing samples, since the plots show a positive zero-intercept. In fact, micropore volumes summarized in Table 4 are large enough to conclude the existence of microprosity in these compounds.

Regarding the ox samples, the specific surface area is reduced with the irradiation time, from 46 $m^2 g^{-1}$ for sample MA-ox-0 to 22 $m^2 g^{-1}$ for sample MA-ox-180. These results agree with the enhancement of the crystallinity of the solids and the growth of the LDH particles.

4. Conclusions

The influence of the microwave–hydrothermal treatment on the ageing of non carbonate-containing LDHs has been studied, to elucidate if the nature of the interlayer anion has any appreciable effect in the ageing process. Two carboxylate anions have been chosen, namely, TA and ox. The ageing process under the influence of the microwave radiation is faster because of the rapid heating, enhancing the dissolution–reprecipitation process. However, some peculiarities are found depending on the anion, TA and ox.

TA-containing samples, both with magnesium or zinc cations in the layers, show a high stability under microwave ageing, as demonstrated by the chemical analyses in which only slight deviations from the values for the unaged sample are obtained. On the other hand, ox samples are not stable and a significant amount of Al^{3+} cations are leached as the irradiation time is increased. Al^{3+} species are supposed to be removed as oxalato complexes, so it seems that the microwave radiation also enhances the side-reaction between the cations and ox species.

The enhancement of the crystallinity in MA-TA and ZA-TA samples follows two well defined trends: while in samples with magnesium it is necessary to extend the irradiation time up to 180 min to reach a high-crystalline degree enhancement, the trend observed for the zinc containing samples is similar to that previously observed for Zn,Al carbonate samples, achieving a well ordered structure in only 10 min and then no additional improvements appears. Another important characteristic of the rapid microwave-heating in the preparation of TA intercalated compounds is that it avoids the presence of interstratified phases, which usually develop after long ageing treatments. In addition, as confirmed by FT-IR spectroscopy, the enhancement of the order also affects to the TA moieties since they achieve a more symmetric coordination. Finally, it should be noticed that microwave treatment also allows cleaning the surface of the solids from some physisorbed organic species.

Acknowledgments

Authors thank financial support from EFRD and MEC (Grant 2006-10800-C02-01). PB acknowledges a grant from Junta de Castilla y León.

Appendix A. Supplementary material

Supplementary data associated with this article can be found in the online version at 10.1016/j.jssc.2008.09.015.

References

[1] V. Rives, in: V. Rives (Ed.), Layered Double Hydroxides: Present and Future, Nova Science Publishers, New York, 2001.
[2] X. Duan, D.G. Evans, Structure and Bonding, Layered Double Hydroxides, vol. 119, 2006.
[3] V. Rives, M.A. Ulibarri, Coord. Chem. Rev. 181 (1999) 61–120.
[4] S.P. Newman, W. Jones, New J. Chem. (1998) 105–115.
[5] V. Prevot, C. Forano, J.P. Besse, Appl. Clay Sci. 18 (2001) 3–15.
[6] P. Benito, F.M. Labajos, J. Rocha, V. Rives, Micropor. Mesopor. Mater. 94 (2006) 148–158.
[7] P. Benito, F.M. Labajos, V. Rives, J. Solid State Chem. 179 (2006) 3784–3797.
[8] M. Herrero, P. Benito, F.M. Labajos, V. Rives, J. Solid State Chem. 180 (2007) 873–884.
[9] M. Herrero, P. Benito, F.M. Labajos, V. Rives, Catal. Today 128 (2007) 129–137.
[10] P. Benito, I. Guinea, F.M. Labajos, J. Rocha, V. Rives, Micropor. Mesopor. Mater. 110 (2008) 292–302.
[11] M.Z.B. Hussein, Z. Zainal, C.Y. Ming, J. Mater. Sci. Lett. 19 (2000) 879–883.
[12] M.A. Drezdzon, Inorg. Chem. 27 (1988) 4628–4632.
[13] A.I. Khan, L. Lei, A.J. Norquist, D. O'Hare, Chem. Commun. (2001) 2342–2343.
[14] V. Ambrogi, G. Fardella, G. Grandolini, L. Perioli, Int. J. Pharm. 220 (2001) 23–32.
[15] S.H. Hwang, Y.S. Han, J.H. Choy, Bull. Korean Chem. Soc. 22 (2001) 1019–1022.
[16] N.T. Whilton, P.J. Vickers, S. Mann, J. Mater. Chem. 7 (1997) 1623–1629.
[17] M. Guenane, C. Forano, J.P. Besse, Mater. Sci. Forum 152 (1994) 343–346.
[18] S.P. Newman, S.J. Williams, P.V. Coveney, W. Jones, J. Phys. Chem. B 102 (1998) 6710–6719.
[19] R.S. Maxwell, R.K. Kukkadapu, J.E. Amonette, H. Cho, J. Phys. Chem. B 103 (1999) 5197–5203.
[20] S.P. Newman, H.C. Greenwell, P.V. Coveney, W. Jones, in: V. Rives (Ed.), Layered Double Hydroxides: Present and Future, Nova Science Publishers, New York, 2001.
[21] A.M. Fogg, A.L. Rohl, G.M. Parkinson, D. O'Hare, Chem. Mater. 11 (1999) 1194–1200.
[22] H.C. Greenwell, W. Jones, S.P. Newman, P.V. Coveney, J. Mol. Struct. 647 (2003) 75–83.
[23] P. Padma Kumar, A.G. Kalinichev, R.J. Kirkpatrick, J. Phys. Chem. B 110 (2006) 3841–3844.
[24] N. Morel-Desrosiers, J. Pissonn, Y. Israëli, C. Taviot-Ghéo, J.P. Besse, J. Mater. Chem. 13 (2003) 2582–2585.
[25] G.R. William, T.G. Dunbar, A.J. Beer, A.M. Fogg, D. O'Hare, J. Mater. Chem. 16 (2006) 1222–1230.
[26] M. Meyn, K. Beneke, G. Lagaly, Inorg. Chem. 29 (1990) 5027–5201.
[27] F. Kooli, I.C. Chisem, M. Vucelic, W. Jones, Chem. Mater. 8 (1996) 1969–1977.
[28] S. Carlino, Solid State Ionics 98 (1997) 73–84.
[29] J. Zhang, F. Zhang, L. Ren, D.G. Evans, X. Duan, Mater. Chem. Phys. 85 (2004) 207–214.
[30] V. Prevot, C. Forano, J.P. Besse, J. Mater. Chem. 9 (1999) 155–160.
[31] P. Beadot, M.E. De Roy, J.P. Besse, Chem. Mater. 16 (2004) 935–945.
[32] M. Vucelic, G.D. Moggridge, W. Jones, J. Phys. Chem. 99 (1995) 8328–8337.
[33] J. Evans, M. Pillinger, J. Zhang, J. Chem. Soc. Dalton Trans. (1996) 2963–2974.
[34] M.R. Weir, J. Moore, R.A. Kydd, Chem. Mater. 9 (1997) 1686–1690.
[35] Y. Guo, D. Li, C. Hu, Y. Wang, E. Wang, Y. Zhou, S. Feng, Appl. Catal. B: Env. 30 (2001) 337–349.

[36] K.M. Parida, S. Parija, J. Das, P.S. Mukherjee, Catal. Commun. 7 (2006) 913–919.
[37] JCPDS: Joint Committee on Powder Diffraction Standards, International Centre for Diffraction Data, Swarthmore, PA, 1977.
[38] V. Rives, Adsorption Sci. Technol. 8 (1991) 95–103.
[39] C. Fernandez, C. Morais, J. Rocha, Solid State NMR 21 (2002) 61–70.
[40] S. Kannan, R.V. Jasra, J. Mater. Chem. 10 (2000) 2311–2314.
[41] J. Rocha, M. del Arco, V. Rives, M.A. Ulibarri, J. Mater. Chem. 9 (1999) 2499–2503.
[42] L. Vieille, E.M. Moujahid, C. Taviot-Guého, J. Cellier, J.-P. Besse, F. Leroux, J. Phys. Chem. Solids 65 (2004) 385–393.
[43] M.A. Ulibarri, F.M. Labajos, V. Rives, R. Trujillano, W. Kagunya, W. Jones, Inorg. Chem. 33 (1994) 2592–2599.
[44] K. Nakamoto, in: Infrared and Raman Spectra of Inorganic Compounds, fourth ed., Wiley, New York, 1986.
[45] F. Wypych, G.G.C. Arízaga, J.E.F.C. Gardolinski, J. Colloid Interface Sci. 283 (2005) 130–138.
[46] F. Rouquerol, J. Rouquerol, K. Sing, in: Adsorption by Powders and Porous Solids. Principles, Methodology and Applications, Academic Press, London, 1999.
[47] H. Nijs, M. de Bock, E.F. Vansant, J. Porous Mater. 6 (1999) 101–110.